Electromagnetic scattering from finite-length metallic carbon nanotubes in the lower IR bands

Jin Hao and George W. Hanson
Department of Electrical Engineering, University of Wisconsin-Milwaukee, 3200 North Cramer Street, Milwaukee, Wisconsin 53211, USA
(Received 23 May 2006; revised manuscript received 21 June 2006; published 27 July 2006)

A model is presented for electromagnetic scattering from infinite planar arrays of finite-length metallic carbon nanotubes, and isolated nanotubes, in the lower IR bands. The scattered field is predicted using a semiclassical formulation based on a periodic Green's function for the array, and a quantum conductance function for the carbon nanotubes. The finite length of the tubes is accounted for electromagnetically by imposing a boundary condition on the tube ends. Scattering characteristics are investigated for various armchair carbon nanotube array configurations, as well as for isolated nanotubes. The principle observations of this study are that longitudinal (end-to-end) coupling between carbon nanotubes is not very important, although transverse (side-to-side) coupling in an array environment shifts and broadens resonance line shapes compared to the isolated tube case. Nanotube length and radius also play critical roles in governing scattering characteristics.

DOI: 10.1103/PhysRevB.74.035119 PACS number(s): 78.67.Ch, 73.25.+i, 42.70.−a, 77.84.Lf

I. INTRODUCTION

The discovery of carbon nanotubes (CN) in 1991 (Ref. 1) has lead to a huge amount of research on their basic properties, and to possible applications in diverse fields. Their unique electrical characteristics have spurred interest in electronic applications such as transistors[2,3] and field emission devices,[4] and there has also been strong interest in their optical and IR properties and possible applications.[5–9]

In this paper we consider electromagnetic scattering from infinite planar arrays of finite-length metallic single-walled carbon nanotubes (SWNTs), and isolated nanotubes. Numerical results are presented for armchair tubes, although zigzag tubes can be analyzed by the same method. Armchair tubes are metallic, with cross-sectional radius $a=3bm/2\pi$ (Ref. 10), where $b=0.142$ nm is the interatomic distance in graphene. In this paper results will be compared between $m=40$ ($a=2.712$ nm), $m=20$ ($a=1.356$ nm), and $m=10$ ($a=0.678$ nm) nanotubes. The model utilized here combines the classical periodic Green's function-integral equation method from electromagnetic theory,[11,12] together with a quantum conductance function for the carbon nanotubes,[13–15] to predict electromagnetic scattering characteristics.

Previously, some fundamental properties of isolated finite-length carbon nanotubes forming dipole antennas were investigated in the GHz, THz, and optical frequency bands.[9,16–19] In Ref. 16 a transmission line model was used, and in Ref. 9 the Leontovich-Levin integrodifferential equation was developed for CNs and applied in the optical range. In Refs. 17–19 a Hallén's-type integral equation was developed for use in the GHz through optical range, and in this paper Hallén's equation is again utilized, with a periodic Green's function to account for array environments. Scattering characteristics are investigated for various armchair carbon nanotube array configurations, as well as for isolated tubes in the lower IR bands. In the considered frequency range it has been previously predicted[17] that isolated finite-length carbon nanotubes will exhibit longitudinal resonances when $2L\simeq\lambda_p/2$, where $2L$ is the tube length and $\lambda_p=\alpha\lambda_0$ is a plasmonic wavelength (λ_0 is the vacuum wavelength), where $\alpha\simeq0.01-0.02$. The analysis in this work shows that broadside mutual coupling in an array environment shifts and broadens the line shape associated with those longitudinal resonances, compared to the isolated tube case. Nanotube length and radius also play critical roles in governing scattering characteristics, and it is shown that relatively large amplitude scattered fields can be obtained from carbon nanotube arrays.

II. FORMULATION OF THE MODEL

Figure 1 depicts an infinite planar array of finite-length carbon nanotubes, where $2L$ is the tube length, D_x and D_z are the interelement separations in the x and z directions, respectively, and a is the radius of each nanotube. For the special case of an isolated carbon nanotube, only the center element is present.

Electromagnetic scattering from this structure is modeled using a Hallén's-type integral equation assuming that the nanotubes are electrically thin ($ka\ll1$) (Ref. 17),

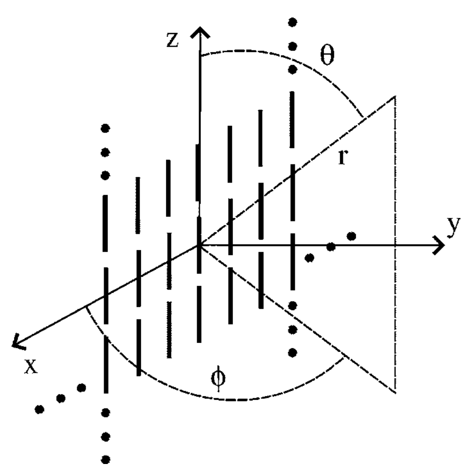

FIG. 1. Infinite planar array of finite-length carbon nanotubes. Each tube has length $2L$, and the array periods along the x and z axes are D_x and D_z, respectively.

$$\int_{-L}^{L}[K(z-z')+q(z-z')]I(z')dz' = c_1 \sin kz + c_2 \cos kz - \frac{j4\pi\omega\varepsilon}{2k}\int_{-\infty}^{\infty}E_z^i(z')\sin k|z-z'|dz' \tag{1}$$

for all $z \in (-L,L)$, where $k=2\pi/\lambda_0$ is the wave number, ω is the radian frequency, ϵ is the permittivity of the material surrounding the tubes (here assumed to be free space), E_z^i is the z component of the incident electric field, $I(z)$ is the unknown current distribution on the center nanotube, c_1 and c_2 are unknown constants to be determined, and $q(z) = 2\pi\omega\varepsilon Z_{cn}e^{-jk|z|}/k$, where $Z_{cn}=(2\pi\sigma_{cn}a)^{-1}$ is the surface impedance of a carbon nanotube, with σ_{cn} being the tube's surface conductance (S).

In (1), $K(z-z')$ is the kernel function, where for an isolated tube

$$K(z-z') = K_{isol}(z-z') = \frac{1}{2\pi}\int_{-\pi}^{\pi}\frac{e^{-jk\sqrt{(z-z')^2+4a^2\sin^2(\phi'/2)}}}{\sqrt{(z-z')^2+4a^2\sin^2(\phi'/2)}}d\phi', \tag{2}$$

and for an infinite planar tube array (Ref. 12)

$$K(z-z') = K_{array}(z-z') = \sum_{m_a=-\infty}^{\infty}\sum_{n_a=-\infty}^{\infty} e^{-jk(m_aP+n_aQ)}\frac{e^{-jkR_{m_an_a}}}{R_{m_an_a}}, \tag{3}$$

where indices m_a and n_a correspond to tube offsets in the x and z directions, respectively, $P=D_x\cos(\phi^i)\sin(\theta^i)$, $Q=D_z\cos(\theta^i)$, θ^i and ϕ^i are the angles of the incident plane wave in the usual spherical coordinates, and $R_{m_an_a}=\sqrt{(m_aD_x)^2+(z-z'-n_aD_z)^2}$; for the center nanotube where $m_a=n_a=0$ we set $R_{00}=\sqrt{(z-z')^2+a^2}$.

Since K_{array} converges very slowly, an accelerated spectral domain form can be derived using Poisson's sum formula and Fourier transforms,[11,12,20] resulting in

$$K_{array} = \frac{2\pi}{D_xD_z}\sum_{m_a=-\infty}^{\infty}\sum_{n_a=-\infty}^{\infty}\left[\left(\frac{1}{K_{ym_an_a}}-\frac{1}{K_{m_an_ap}}\right)\times e^{-j[((2n_a\pi/D_z)+(kQ/D_z))(z-z')]}\right] + \sum_{m_a=-\infty}^{\infty}\sum_{n_a=-\infty}^{\infty} e^{-jk(m_aP+n_aQ)}\frac{e^{-u_aR_{m_an_a}}}{R_{m_an_a}}, \tag{4}$$

where $K_{ym_an_a}=\sqrt{|K_{sm_an_a}|^2-k^2}$, $K^2_{m_an_ap}=|K_{sm_an_a}|^2+u_a^2$, and $|K_{sm_an_a}|^2=(2m_a\pi/D_x+kP/D_x)^2+(2n_a\pi/D_z+kQ/D_z)^2$. The constant u_a is chosen to be one-half the size of the maximum reciprocal lattice base vector in order to obtain fast convergence,[20] $u_a=\pi\sqrt{D_x^{-2}+D_z^{-2}}$.

The fact that we are modeling carbon nanotubes is represented by the surface impedance Z_{cn} through the conductance σ_{cn} (the model can be applied to imperfect metallic wires by replacing Z_{cn} with the appropriate metal surface impedance[17]). For an armchair or zigzag carbon nanotube the quantum conductance is given by (Refs. 13–15)

$$\sigma_{cn}(\omega) = \frac{je^2\omega}{\pi^2\hbar a}\left\{\frac{1}{\omega(\omega-j\nu)}\sum_{s=1}^{m}\int_{1stBZ}\frac{\partial F_c}{\partial p_z}\frac{\partial \mathcal{E}_c}{\partial p_z}dp_z + 2\sum_{s=1}^{m}\int_{1stBZ}\mathcal{E}_c|R_{vc}|^2\frac{F_c-F_v}{\hbar^2\omega(\omega-j\nu)-4\mathcal{E}_c^2}dp_z\right\}, \tag{5}$$

where e is the charge of an electron, $\nu=\tau^{-1}$ is the phenomenological relaxation frequency (τ being the relaxation time), $\hbar$ is the reduced Planck's constant, $F_{c,v}$ and $\mathcal{E}_{c,v}$ are the equilibrium Fermi distribution function and electron dispersion relation in the conduction or valance bands, respectively, and R_{vc} is the matrix element for the tube. Explicit expressions for these quantities are given in Ref. 15.

In the low and middle IR regime considered here, below optical interband transitions, (5) reduces to the simple expression (Refs. 13 and 14)

$$\sigma_{cn}(\omega) \simeq -j\frac{2e^2v_F}{\pi^2\hbar a(\omega-j\nu)}, \tag{6}$$

where $v_F=3\gamma_0 b/2\hbar$ is the Fermi velocity for a CN. At low and middle IR frequencies $\gamma_0 \simeq 2.7$ eV (Ref. 21) and $\tau \simeq 3$ ps, in accordance with low-frequency measurements.[13] Note that the units of σ_{cn} are siemens (S) since the CN is modeled as an infinitely thin tube supporting a surface current density.

The current distribution on the center tube is determined by solving (1). Here we use the method of moments.[22] The unknown current I is expanded in a set of pulse functions

$$I(z) = \sum_{n_p=1}^{N} I_{n_p}P_{n_p}(z), \tag{7}$$

where $P_{n_p}(z)=1$ if $z_{n_p}-\Delta/2 \le z \le z_{n_p}+\Delta/2$, and $P_{n_p}(z)=0$ otherwise, where $z_{n_p}=-L+(n_p-\frac{1}{2})\Delta$ with Δ being the pulse

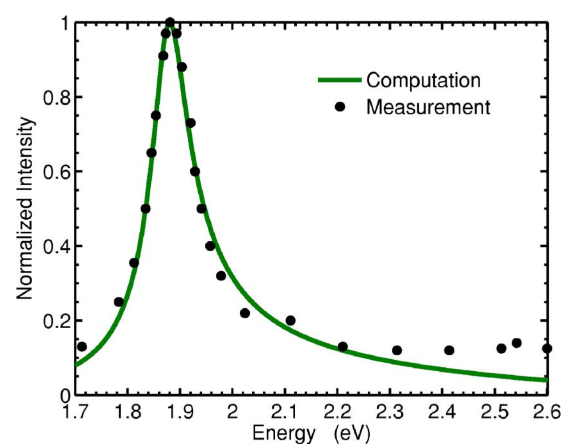

FIG. 2. (Color online) Comparison between Rayleigh scattering measurements (Ref. 25) and simulation [computed using (1)] for an $a=0.678$ nm carbon nanotube ($m=10$). The simulation used $\tau=0.0098$ ps and $\gamma_0=3.03$ eV.

width, $\Delta = 2L/N$. Testing at points $z = z_{m_t}$, $m_t = 1, 2, \ldots, N$ and enforcing $I(1) = I(N) = 0$ (current must vanish at the tube ends) leads to an $N \times N$ system of equations from which the pulse amplitudes I_{n_p} can be obtained. By applying Floquet's theorem[23] all of the current distributions on the other array elements are obtained by phase shifting from the center tube.

After the currents are determined the far scattered electric field can be found. For an isolated nanotube in the far field $\mathbf{E} = \hat{\boldsymbol{\theta}} E_\theta$, where (Ref. 24)

$$E_\theta^s(r,\theta) = j\omega\mu_0 \frac{e^{-jkr}}{4\pi r} \int_{-L}^{L} I(z') e^{jkz' \cos\theta} dz' \quad (8)$$

and where r is the radial distance from the origin (in this case the tube center). For an infinite array (Ref. 12),

$$d\mathbf{E}^s(r,\theta,\phi,z') = dz' I_{00} \frac{jkZ_c}{2D_x D_z} \sum_{m_a=-\infty}^{\infty} \sum_{n_a=-\infty}^{\infty} \frac{e^{-r \sin\theta \sin\phi K_{y m_a n_a}}}{K_{y m_a n_a}} \cdot e^{-j[((2m_a\pi)/(D_x)+(kP)/(D_x)) r \sin\theta \cos\phi + ((2n_a\pi)/D_z + (kQ/D_z))(r\cos\theta - z')]} \cdot \mathbf{e}_{m_a n_a}, \quad (9)$$

for $0 < \phi < \pi$, where I_{00} is the current distribution on the center nanotube, $Z_c = \sqrt{\mu_0/\varepsilon_0} \simeq 377\ \Omega$ is the wave impedance of free space, and

$$\mathbf{e}_{m_a n_a} = \hat{\mathbf{x}} V_x V_z + \hat{\mathbf{y}} V_z V_y - \hat{\mathbf{z}}(1 - V_z^2), \quad (10)$$

where $V_x = P/D_x + m_a \lambda / D_x$, $V_z = Q/D_z + n_a \lambda / D_z$, and $V_y = \sqrt{1 - V_x^2 - V_z^2}$. The total scattered field $\mathbf{E}^s$ can be obtained from (9) as follows:

$$\mathbf{E}^s(r,\theta,\phi) = \int_{-L}^{L} d\mathbf{E}^s(r,\theta,\phi,z'). \quad (11)$$

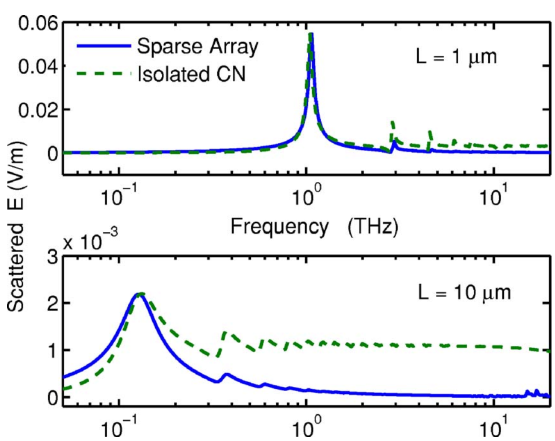

FIG. 3. (Color online) Scattering characteristics of $L = 1$ μm and $L = 10$ μm armchair tubes having $a = 2.712$ nm ($m = 40$). Results for isolated tubes are shown, along with those for relatively sparse infinite arrays (for $L = 1$ μm, $D_x = 1$ μm, and $D_z = 3$ μm, and for $L = 10$ μm, $D_x = 20$ μm, and $Dz = 40$ μm). The amplitude scale is for the array result; the isolated tube results have been normalized to align with peak array amplitudes to facilitate comparisons. For the $L = 1$ μm isolated tube, $E_{peak} = 6.209 \times 10^{-6}$ V/m (at $f = 1.047$ THz), and for the $L = 10$ μm isolated tube, $E_{peak} = 7.66 \times 10^{-6}$ V/m (at $f = 0.1318$ THz).

III. VERIFICATION OF THE MODEL

The presented model was verified in several ways. Although limited electromagnetic scattering results are available for carbon nanotubes, there is one recent Rayleigh scattering measurement of a metallic tube where the tube geometry could be unambiguously specified.[25] In this case, concerning an isolated $a = 0.678$ nm ($m = 10$) armchair nanotube, the scattered field predicted from (1) is in excellent agreement with the measured result, as shown in Fig. 2. Regarding this agreement, however, it must be noted that the tight-binding conductance model (5) or (6) contains two adjustable parameters, the relaxation time τ and the overlap integral γ_0 [in (5), γ_0 is contained in $\mathcal{E}_{c,v}$ and R_{vc}]. As discussed in detail in Ref. 19, in the optical range τ is approximately 0.01 ps (τ is reduced from the low-frequency value of 3 ps by electron interactions with optical phonons) and $\gamma_0 \simeq 3.03$ eV, and so the excellent agreement shown in Fig. 2 corresponds to an appropriate choice of these parameters. Furthermore, the measured results shown in Fig. 2 are for a

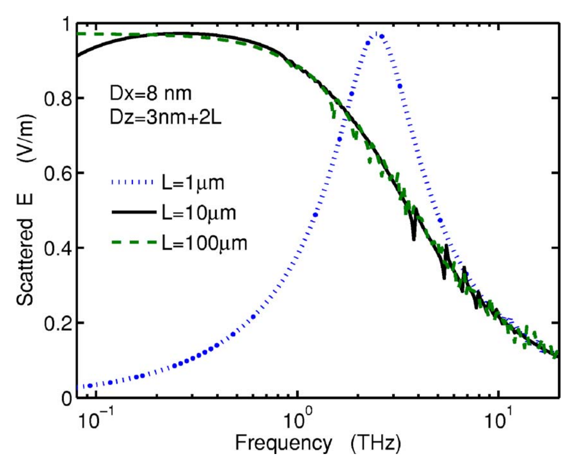

FIG. 4. (Color online) Scattering characteristics of infinite planar arrays of $L = 1$, 10, and 100 μm armchair tubes having $a = 2.712$ nm ($m = 40$).

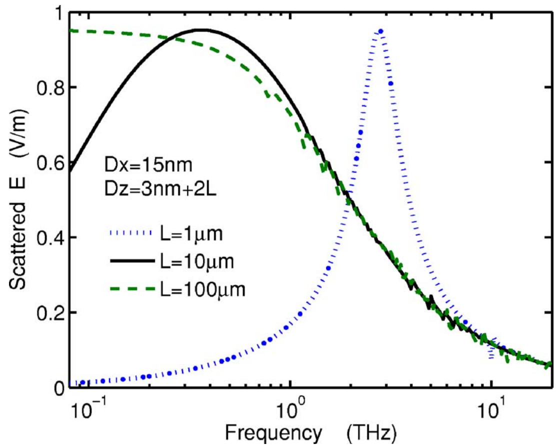

FIG. 5. (Color online) Scattering characteristics of infinite planar arrays of $L=1$, 10, and 100 μm armchair tubes having $a=2.712$ nm ($m=40$). Broadside interelement spacing is larger than in Fig. 4.

25 μm long tube illuminated over a 2 μm spot.[25] As discussed in Ref. 19, in the optical range current is strongly damped on the tube, and so the resonance shown in the figure is due to the electronic structure of the tube (interband transitions), and is not due to tube-length-dependent longitudinal current resonances. However, in the lower THz regime considered in the following there are no interband transitions, and resonances are in fact due to the finite length of the tubes.

Furthermore, as described in Ref. 17, for an isolated tube the integral equation (1) and its solution was used to reproduce known results (for current distribution, input impedance, scattered field, etc.) for an imperfect metal conductor upon replacing Z_{cn} for the carbon nanotube with the surface impedance of the metal.

To verify the array formulation, for the case of perfectly conducting wires the current distribution on the center wire was found to agree well with the results presented in Refs. 11 and 26, and the predicted far-scattered field agreed with results in Ref. 27. As a further check, results from the infinite planar array were found to agree with those for an isolated nanotube as D_x and D_z became very large.

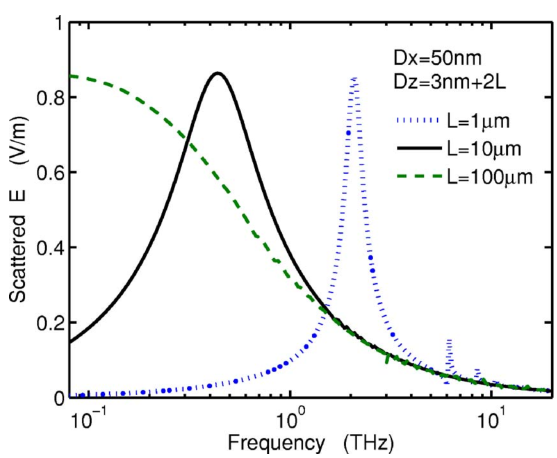

FIG. 6. (Color online) Scattering characteristics of infinite planar arrays of $L=1$, 10, and 100 μm armchair tubes having $a=2.712$ nm ($m=40$). Broadside interelement spacing is larger than in Figs. 4 and 5.

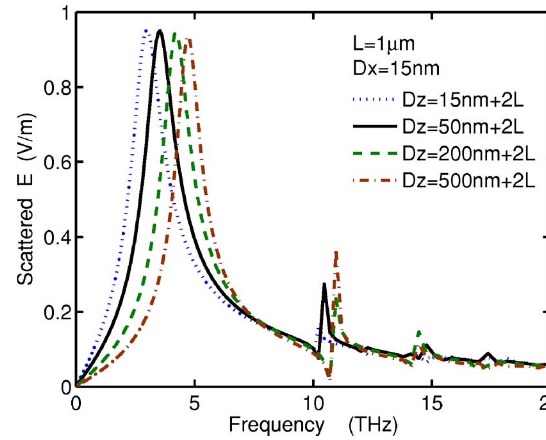

FIG. 7. (Color online) Scattering characteristics of infinite planar arrays of $L=1$ μm armchair tubes having $a=2.712$ nm ($m=40$), showing the effect of end-to-end mutual coupling.

IV. RESULTS

For a macroscopic planar array of metallic wires, when $\theta^i=0°$ the z component of the incident and scattered is zero, and when $\theta^i=90°$, $\mathbf{E}^i=\hat{\mathbf{z}}E_z^i$, and $\mathbf{E}^s\simeq\hat{\boldsymbol{\theta}}E_\theta^s$ approaches its maximum. In the latter case the scattered field E_θ^s is slightly dependent on incident angle ϕ^i. For the carbon nanotube array similar behavior was found. In the following results incidence angles are $\theta^i=90°$, $\phi^i=30°$, and observation angles are $\theta=90°$, $\phi=150°$, and $E_z^i=1$ V/m.

From (9), it can be observed that the field from an array of Hertzian elements consists of an infinite number of plane waves, and that their directions are determined by $\mathbf{e}_{m_a n_a}$. When $|K_{sm_a n_a}|^2-k^2<0$ (which occurs for the first few terms), the plane waves will propagate away from the array without attenuation. However, when $|K_{sm_a n_a}|^2-k^2>0$ the plane waves

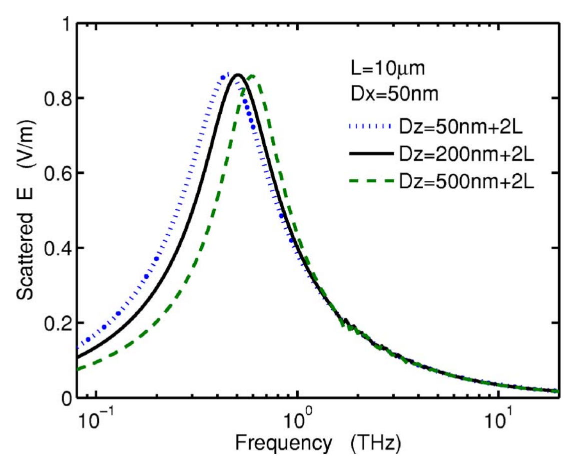

FIG. 8. (Color online) Scattering characteristics of infinite planar arrays of $L=10$ μm armchair tubes having $a=2.712$ nm ($m=40$), showing the effect of end-to-end mutual coupling.

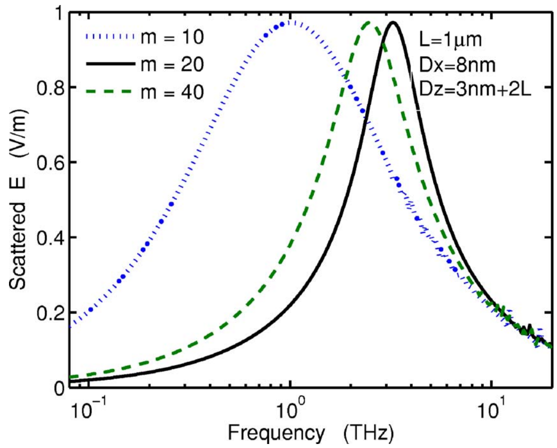

FIG. 9. (Color online) Scattering characteristics of infinite planar arrays of $L=1$ μm armchair tubes having different radius values.

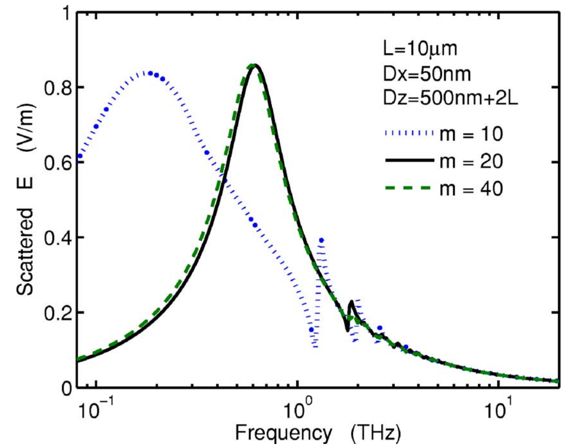

FIG. 10. (Color online) Scattering characteristics of infinite planar arrays of $L=10$ μm armchair tubes having different radius values.

are evanescent, and are attenuated more strongly as the point of observation moves away from the array in the direction of the array normal (i.e., along the y coordinate). Therefore, if the observation point is far enough from the array the scattered electric field will be independent of y. Since $y=r\sin(150°)$, we have determined that having $r \geq 100$ μm ($y \geq 50$ μm) is far enough to attenuate all evanescent waves and have a distance-independent scattered field. Thus, in all of the results reported here the observation point is $(r,\theta,\phi)=(100\ \mu\text{m},90°,150°)$, although the same results would be obtained for larger values of r. As a practical matter in performing measurements on finite arrays, one should have $r>100$ μm but $r<L_x,L_z$, where L_x,L_z represent the finite extent of the array. Furthermore, in the following results the quantity $E=|\mathbf{E}^s| \simeq |E_\theta^s|$ is plotted.

For an isolated armchair tube having $a=2.712$ nm ($m=40$), Fig. 3 shows scattering characteristics of $L=1$ μm and $L=10$ μm tubes. Results for isolated tubes are shown, along with those for relatively sparse infinite arrays, where in the array case $D_x=1$ μm and $D_z=3$ μm for the $L=1$ μm tube, and $D_x=20$ μm and $Dz=40$ μm for the $L=10$ μm tube.

For both the sparse array and isolated tube cases, in the considered frequency range current resonances associated with the finite-length of the tubes are present. As discussed in Ref. 17, for an isolated $L=10$ μm tube the first resonance occurs at $f \simeq 160$ GHz. The current distribution at this frequency is approximately a half-wave sinusoid, and thus $2L=\lambda_p/2$, or $\lambda_p=4L=40$ μm, where λ_p is the wavelength of the plasma oscillation along the tube. Writing $\lambda_p=\alpha\lambda_0$, then $\alpha \simeq 0.02$. Therefore, longitudinal current resonances due to the finite length of the tube occur, but at tube lengths approximately 50 times smaller than would be found for a perfectly conducting tube. For the $L=1$ μm tube the fundamental current resonance occurs at $f \simeq 1.3$ THz, and $\alpha \simeq 0.017$.

In the array cases shown in Fig. 3 these current resonances are relatively unaffected by mutual coupling among tubes, since the tubes are widely separated. However, the scattered field amplitude is much larger for an array then for an isolated tube, and in Fig. 3 the vertical axis corresponds to the array result. The scattered field amplitudes for the isolated tubes have been normalized to align with the array peak values, although the peak amplitudes for the isolated cases are given in the figure captions.

For arrays with closer interelement spacings, mutual coupling significantly influences scattering characteristics. For armchair tubes having $a=2.712$ nm ($m=40$), Fig. 4 shows the scattered field as a function of frequency for interelement spacings $D_x=8$ nm and $D_z=3$ nm$+2L$, and element lengths $L=1$ μm, $L=10$ μm, and $L=100$ μm. It can be seen that in each case the fundamental current resonance shown in Fig. 3 has been significantly blueshifted and broadened by mutual coupling. For the $L=1$ μm and $L=10$ μm tubes in this array environment, the resonances occur at approximately 2.6 and 0.3 THz, respectively.

Figures 5 and 6 show the scattered field when the broadside interelement spacing D_x is increased to 15 and 50 nm, respectively, again for $D_z=3$ nm$+2L$. It is found that as D_x increases the current resonance linewidth narrows toward the isolated tube case, and the resonance frequency also tends to the isolated case, although not monotonically. This is consistent with known array effects, where broadside mutual coupling decreases in an oscillatory fashion as spacing increases (Ref. 24, Sec. 7.13).

Since carbon nanotubes tend to radiate broadside and not along the tube axis,[17] one would expect that end-to-end mutual coupling effects are less significant than broadside coupling. Figures 7 and 8 show scattering characteristics for several D_z values for $L=1$ μm and $L=10$ μm element arrays, respectively. From the figures it can be seen that end-to-end coupling does play a role in scattering behavior, but is not nearly as significant as broadside coupling. This is also consistent with known results for metal wires.[24]

Figures 9 and 10 show a comparison between different radius carbon nanotubes [$a=2.712$ nm ($m=40$), $a=1.356$ nm ($m=20$), and $a=0.678$ nm ($m=10$)] having half-lengths $L=1$ μm and $L=10$ μm, respectively. In Fig. 9 interelement spacings are relatively small, and in Fig. 10 interelement spacings are much larger, although both plots show that the influence of radius is quite pronounced, especially between the $a=0.678$ nm and $a=2.712$ nm tubes.

V. CONCLUSIONS

Electromagnetic scattering characteristics of infinite planar arrays of finite-length armchair carbon nanotubes, and isolated nanotubes, have been investigated using an integral equation technique. The tubes are modeled using a quantum mechanical conductance, and results are presented in the lower and middle IR bands. It has been found that the resonance line shape of isolated tubes is broadened and shifted for tubes in an array environment. Broadside mutual coupling is found to be more significant than end-to-end coupling, similar to the case of ordinary metallic wires.

[1] I. Iijima, Nature (London) **354**, 56 (1991).
[2] S. Li, Z. Yu, S. F. Yen, W. C. Tang, and P. J. Burke, Nano Lett. **4**, 753 (2004).
[3] J. P. Clifford, D. L. John, L. C. Castro, and D. L. Pulfrey, IEEE Trans. Nanotechnol. **3**, 281 (2004).
[4] G. Pirio, P. Legagneux, D. Pribat, K. B. K. Teo, M. Chhowalla, G. A. J. Amaratunga, and W. I. Milne, Nanotechnology **13**, 1 (2002).
[5] Z. Yu and P. J. Burke, Nano Lett. **5**, 1403 (2005).
[6] Y. Wang, K. Kempa, B. Kimball, J. B. Carlson, G. Benham, W. Z. Li, T. Kempa, J. Rybczynski, A. Herczynski, and Z. F. Ren, Appl. Phys. Lett. **85**, 2607 (2004).
[7] G. Y. Guo, K. C. Chu, D.-S. Wang, and C.-G. Duan, Phys. Rev. B **69**, 205416 (2004).
[8] V. N. Popov and L. Henrard, Phys. Rev. B **70**, 115407 (2004).
[9] G. Ya. Slepyan, M. V. Shuba, S. A. Maksimenko, and A. Lakhtakia, Phys. Rev. B **73**, 195416 (2006).
[10] R. Saito, G. Dresselhaus, and M. S. Dresselhaus, *Physical Properties of Carbon Nanotubes* (Imperial College Press, London, 2003).
[11] V. W. H. Chang, Proc. IEEE **56**, 1892 (1968).
[12] B. A. Munk and G. A. Burrell, IEEE Trans. Antennas Propag. **27**, 331 (1979).
[13] G. Y. Slepyan, S. A. Maksimenko, A. Lakhtakia, O. Yevtushenko, and A. V. Gusakov, Phys. Rev. B **60**, 17136 (1999).
[14] S. A. Maksimenko and G. Y. Slepyan, in *Electromagnetic Fields in Unconventional Materials and Structures*, edited by O. N. Singh and A. Lakhtakia (Wiley, New York, 2000).
[15] S. A. Maksimenko and G. Y. Slepyan, in *The Handbook of Nanotechnology-Nanometer Structures/Theory, Modeling, and Simulation*, edited by A. Lakhtakia (SPIE Press, Bellingham, 2004).
[16] P. J. Burke, S. Li, and Z. Yu, available at http://xxx.lanl.gov/abs/cond-mat/0408418 (unpublished).
[17] G. W. Hanson, IEEE Trans. Antennas Propag. **53**, 3426 (2005).
[18] G. W. Hanson, IEEE Trans. Antennas Propag. **54**, 76 (2006).
[19] J. Hao and G. W. Hanson (unpublished).
[20] S. Singh, W. Richards, J. R. Zinecker, and D. R. Wilton, IEEE Trans. Antennas Propag. **38**, 1958 (1990).
[21] J. W. G. Wildöer, L. C. Venema, A. G. Rinzler, R. E. Smalley, and C. Dekker, Nature (London) **391**, 59 (1998).
[22] A. F. Peterson, S. L. Ray, and R. Mittra, *Computational Methods for Electromagnetics* (Wiley-IEEE Press, New Jersey, 1997).
[23] L. Brillouin, *Wave Propagation in Periodic Structures* (Dover, New York, 1953).
[24] R. S. Elliott, *Antenna Theory and Design* (Prentice-Hall, New Jersey, 1981).
[25] M. Y. Sfeir, T. Beetz, F. Wang, L. Huang, X. M. H. Huang, M. Huang, J. Hone, S. O'Brien, J. A. Misewich, T. F. Heinz, L. Wu, Y. Zhu, and L. E. Brus, Science **312**, 554 (2006).
[26] A. L. VanKoughnett and J. L. Yen, IEEE Trans. Antennas Propag. **15**, 750 (1967).
[27] M. Joseph and B. A. Munk, IEEE Trans. Antennas Propag. **42**, 946 (1994).